PRAMANA
— journal of
physics

Vol. 54, No. 5
May 2000
pp. 685–708

Pressure induced phase transition behaviour in f-electron based dialuminides

P CH SAHU and N V CHANDRA SHEKAR
Materials Science Division, Indira Gandhi Centre for Atomic Research, Kalpakkam 603 102, India
Email: padma@igcar.ernet.in

MS received 20 September 1999; revised 7 March 2000

Abstract. The rare-earth and actinide based compounds are endowed with several exotic physical and chemical properties due to the presence of f-electrons. These properties exhibit interesting changes under the action of various thermodynamic fields and hence continues to be a subject of extensive research. For instance, under pressure, the nature of f-electrons can be changed from localized to itinerant, leading to a variety of changes in their structural, physical and chemical properties. The present review on the high pressure phase transition behaviour of dialuminides of rare earths and actinides is an outcome of research in our laboratory during the last five years using a unique combination of a Guinier diffractometer and a diamond anvil cell built in-house. To bring out the correlations between the compressibility and structural behaviour with the electronic structure, we have also carried out electronic structure calculation. Further, the usefulness of Villars' three parameter structure maps in predicting pressure induced structural transitions has been explored and this has been illustrated with the available phase transition data.

Keywords. High pressure; x-ray diffraction; actinides and rare-earths; dialuminides; phase transition.

PACS Nos 61.10.My; 62.50.+p; 61.66Fn; 64.30.+t; 64.70.Kb

1. Pressure in condensed matter physics

Pressure and temperature are two important thermodynamic variables to study condensed matter. Compared to temperature, pressure induces more pronounced changes in their physical and chemical properties [1]. The effect of pressure on materials can broadly be classified into two categories, namely, the lattice compression and the electronic structure change. However, these two changes are not totally independent and often one is associated with the other.

The decrease in interatomic distances or increase in the density leading to changes in the phonon spectra, increase in the free energy (G) and the associated phase transitions stabilizing compact structures characterized by significant changes in the physical properties come under 'lattice effects'.

As the interatomic distance decreases, the overlap of outer electronic orbitals increases leading to an increase in the band widths, the extent of hybridization of the outer electronic

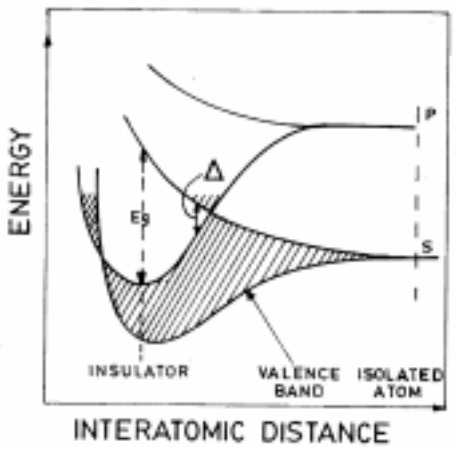

Figure 1. Schematic of the electronic energy band versus interatomic distance. Broadening and shifting of various bands with respect to the Fermi energy E_{F} can be noticed. In the figure, p and s denote the electron state and Δ is the hopping energy.

orbitals, shifting of energy bands as well as the Fermi energy (E_{F}) (figure 1). All these electronic effects lead to interesting changes in their physical and chemical properties [2,3]. For instance, closing of energy gaps lead to metal–insulator transitions [4], shift in energy bands lead to interband electron and valence transitions [5], change in the topology of the Fermi surface lead to Lifshitz type transitions [6] and so forth. As a consequence, these effects are reflected well in their physical properties such as electronic specific heat, superconductivity and magnetism.

2. Pressure induced behaviour of f-electron based systems: Background and motivations

Pressure plays a significant role in studying the nature of f-electron based lanthanide ($4f$) and actinide ($5f$) systems. It may be recalled that at STP in the lanthanide elements, the $4f$ states are localized and magnetic, whereas in actinides the $5f$ states exhibit dual nature [2,7]. That is, in early actinides, (up to Pu), the $5f$ states are itinerant and non-magnetic whereas in late actinides (Am and above), the $5f$ states are lanthanide-like, viz., localized. Most of their physical properties are governed by the nature of their f-electron states [7,8]. For instance, the systems with itinerant f-electron states exhibit complex anisotropic physical properties, higher bulk modulus and stabilize in low symmetry crystal structures. On the other hand, localized f-electron based systems exhibit local magnetic moments, low bulk modulus and adopt in high symmetry crystal structures. The itinerant f-electron based systems show higher bulk modulus as the f-electron states participate in bonding and strengthen the lattice. As the nature of f-electron states depend on the f-orbital overlaps, these can be tuned in a controlled manner by changing the interatomic distances [7] by applying external pressure. This influences the physical properties of the f-electron based systems and studies on pressure effects in these systems appears to be quite exciting [9].

Since the electronic structure determines the ground state atomic arrangements [7], studies on crystal structures provide valuable information on the underlying electronic structure. A systematic study of the pressure induced structural sequences has become very important in probing their electronic structure, in understanding the transition mechanisms and in predicting phase transitions [2,3]. However, the radioactivity of the actinide systems puts severe restrictions in handling and investigating their properties. Laboratories equipped with glove boxes for handling radioactive materials are required for preparing the actinide samples and loading it in a high pressure cell.

The pressure induced structural studies on almost all the available f-electron elements have been carried out and their observed systematic behaviour has been understood with respect to the nature and occupations of the f-electron states [2,10]. However, as far as their compounds are concerned, very little progress has been made [3]. The only group of compounds which have been studied to some extent leading to certain structural systematics is the AB type. They transform from B1 (NaCl type) to B2 (CsCl type) structures under pressure [2]. Among the AB_2 type compounds, some of the dioxides transform from the C1 (CaF_2 type) to the $PbCl_2$ type structures under pressure [2]. However, no such systematic studies have been done on their AB_2 type intermetallic compounds. Table 1 lists some of the AB_2 type intermetallics which have been studied under high pressure so far [11–18]. Out of the 12 systems studied, only 3 of them show structural transitions.

With this motivation, we have carried out the high pressure x-ray diffraction studies on the AB_2 type intermetallics of the f-electron systems, especially the dialuminides for their structural investigations under pressure. Also, to understand the observed behaviour, we have performed structural stability and electronic structure calculations using the tight binding-linearized muffin tin orbital (TB-LMTO) method. The compressibility and structural systematics that have evolved have been highlighted and their correlation with the electronic structure has been brought out. The usefulness of Villars' three parameter structure stability maps [19] in predicting pressure induced phase transitions have been elucidated. The review is mostly based on the work carried out in our laboratory and wherever necessary, relevant work has been drawn from the literature.

Table 1. Isothermal bulk modulus B_0 (GPa) and high pressure structures for f electron based AB_2 type intermetallic compounds as determined from high-pressure x-ray diffraction (n.d.: not determined).

f electron compd.	Structure type at NTP	$P_{\max}$ GPa	B_0 GPa	High pressure structure. The transition pressures are given in the bracket	Refs
$ThAl_2$	AlB_2	30	71	$ZrSi_2$(12), $ThSi_2$(22)	[11]
UAl_2	$MgCu_2$	50	83	$MgNi_2$(12)	[12,13]
UMn_2	$MgCu_2$	42	320	–	[14]
UFe_2	$MgCu_2$	48	239	–	[14]
UCo_2	$MgCu_2$	35	217	–	[14]
Ulr_2	$MgCu_2$	50	290	–	[14]
$CeAl_2$	$MgCu_2$	23	234	–	[15]
$GdAl_2$	$MgCu_2$	16	69	–	[15]
$LaAl_2$	$MgCu_2$	15	n.d.	–	[16]
$PrAl_2$	$MgCu_2$	3.7	102	–	[17]
$YbAl_2$	$MgCu_2$	3.5	79	–	[17]
$TmGa_2$	$CeCu_2$	45	95	AlB_2(21)	[18]

3. Experimental details

The dialuminides of La, Ce and Gd from the lanthanide group and that of Th and U from the actinide group were prepared by arc-melting method and were characterized by x-ray diffraction (XRD) using a high precision Guinier diffractometer [20,21]. All the samples were found to be in single phase and the lattice parameters matched well with standard values available in the respective *powder diffraction files* provided by the International Centre for Diffraction Data.

High pressure x-ray diffraction (HPXRD) was carried out in the angle dispersive mode by using a Mao–Bell type diamond anvil cell (DAC) and a Guinier diffractometer. The schematic of the system is shown in figure 2. The DAC capable of generating pressure up to ~ 50 GPa was developed in our Centre [21,22]. A mixture of methanol, ethanol and water (MEW) in the ratio of $16:3:1$, was used as the pressure transmitting medium. Either the equation of state (EOS) of Ag [23] or the ruby fluorescence method [24] was employed for determining the sample pressure. The incident Mo x-ray obtained from a Rigaku 18 kW rotating anode x-ray generator, was monochromatized by a curved crystal monochromator and an almost pure $K_{\alpha 1}$ beam was impinged on the sample. A flat position sensitive detector (PSD) was used for detecting the diffracted x-rays. Apart from the pure $K_{\alpha 1}$ radiation which ensures clear XRD patterns with very good signal to noise ratio, there are two more important added advantages with this system, namely, (i) due to focussing of the diffracted beam, the photon flux on the detector gets enhanced by at least 2 orders in magnitude, and (ii) the spatial resolution is 2 times better compared to the Debye–Scherrer geometry. As a result, it is possible to obtain high resolution synchrotron quality

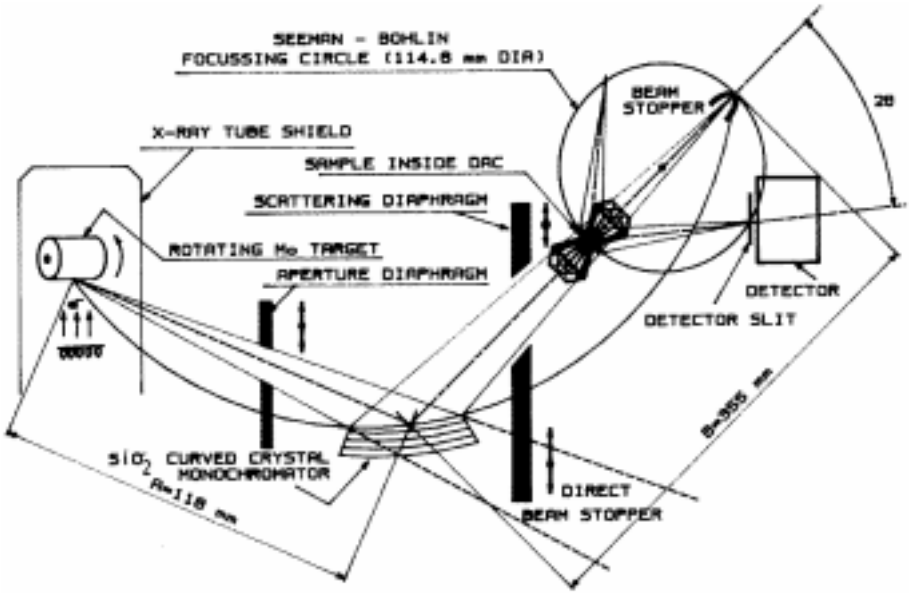

Figure 2. Schematic of the angle dispersive x-ray diffraction setup in the Guinier geometry for performing high-pressure experiments using a DAC [20].

HPXRD patterns within 30 min with this instrumentation. However, due to the use of a flat PSD in the present set up, the overall resolution of the HPXRD data has been found to be $\Delta d/d \sim 0.015 \pm 0.005$. This can further be improved by using a curved PSD. The capability of this instrumentation can be judged from the fact that, in earlier synchrotron based HPXRD experiments, UAl_2 and BaFCl were observed to undergo structural phase transitions, but the data quality were not good enough to characterize the structures of the high pressure phases. Using our instrumentation, it was possible to identify the crystal structures of the high pressure phases of both UAl_2 and BaFCl [12,13,25].

4. f-electron based dialuminides: Present investigations

4.1 *The U–Al systems*

There are three known intermetallics in this system viz., UAl_2, UAl_3 and UAl_4. Although our aim was to investigate UAl_2, the other two systems were also taken up for the purpose of comparing the nature of the $5f$ states in the U–Al systems. UAl_2 shows spin fluctuation behavior [26] and has been studied extensively by various techniques. However, very little information is available on the other two compounds. The low temperature specific heat [27], magnetic susceptibility [28–30] and electrical resistivity studies [29,31] on UAl_2 clearly indicate ferromagnetic type spin fluctuation behaviour.

Hill plots [32] played a key role in predicting the nature of f-electrons in these systems. These plots are empirical in nature and divide the f-electron based compounds into two groups: one with itinerant f-electrons and the other with localized on the basis of their increasing interactinide ion distances d_{An}. For uranium compounds, the transition zone is at $d_{\mathrm{An}} \sim 3.5$ Å. UAl_2 has a cubic $MgCu_2$ type structure (s.g. Fd3m) with $d_{\mathrm{An}} \sim 3.38$ Å, very close to the Hill limit. Photoemission studies [33] indicate itinerant nature of the $5f$ electron states in this system. UAl_3 has a simple cubic structure (s.g. Pm3m) with $d_{\mathrm{An}} \sim 4.27$Å, much above the Hill limit. UAl_4 on the other hand has an orthorhombic structure (s.g. Imma) with $d_{\mathrm{An}} \sim 4.37$ Å, also above the Hill limit. Thus it is expected that these two systems should have localized $5f$-electron states as per the Hill criterion. However, some exceptions have been found to exist. There are systems like UGe_3, USn_3 and $NpSn_3$ in which the $5f$-electron states are itinerant although their d_{An} values are much above the Hill limit [34]. This has been attributed to the strong hybridization of the $5f$ orbitals with that of the other constituent atoms [35]. Low temperature electrical resistivity and magnetic susceptibility studies on UAl_3 and UAl_4 indicate localized spin fluctuation behaviour. However, magnetic susceptibility and specific heat measurements by Van Maaren *et al* [36] on UAl_3 and by Mielke *et al* [37] on UAl_4 indicate more towards itinerant nature of their $5f$ states. In UAl_2, high pressure magnetic susceptibility [38] and electrical resistivity [39] studies show suppression of spin-fluctuation under pressure. With this background, the above three systems were studied and the results are discussed in the following subsections.

4.1.1. *Compressibility behaviour:* The high pressure X-ray diffraction pattern of UAl_3 and UAl_4 are shown in figures 3 and 4 respectively. There are no major changes in the patterns, but systematic shift of the diffraction peaks to higher Bragg angles as a function of pressure

can be noticed. UAl_2 shows a structural phase transition at ~ 11 GPa and this is discussed in detail in the subsequent section.

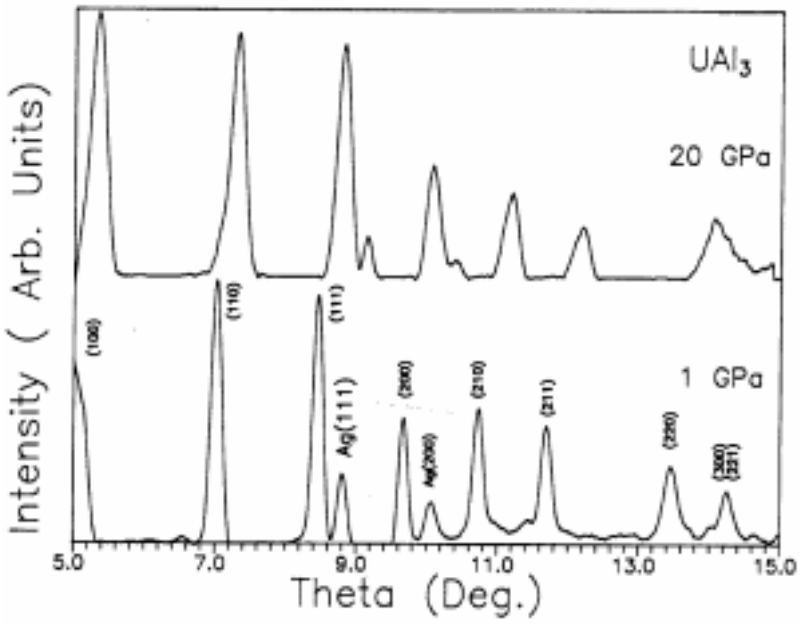

Figure 3. High pressure x-ray diffraction patterns of UAl_3 at 1 GPa and 20 GPa. Molybdenum $K_{\alpha 1}$ radiation with $\lambda = 0.709\,26$ Å was used. Silver was used as the internal pressure calibrant [12].

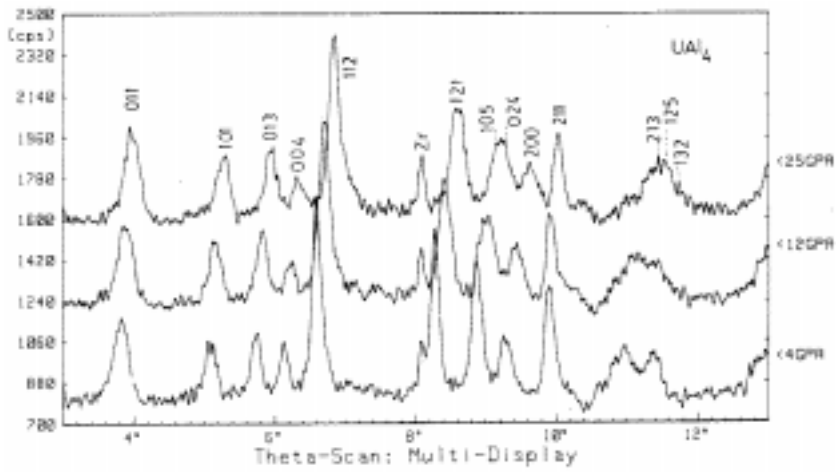

Figure 4. High pressure x-ray diffraction spectra of UAl_4 [13].

The P–V data for UAl_2, UAl_3 and UAl_4 are shown in figure 5. In figure 5, the P–V data for UAl_3 obtained by recording the HPXRD patterns on x-ray films is shown. Subsequently, high resolution P–V data for UAl_3 were obtained using the Guinier diffractometer and is shown in figure 6. The P–V curve of UAl_3 shown in figure 6, compares very well with those reported for similar compounds such as, UGa_3 and UIn_3 [41]. The curve shows clearly some change in the slope at about 5 and 10 GPa. The P–V data shown in figure 5 were fitted to both the Murnaghan and the Birch–Murnaghan equation of state (EOS) to obtain the bulk modulus B_0 and its pressure derivative B_0' which are listed in table 2. The EOSs generally used in the high pressure work are due to Murnaghan [42] and Birch–Murnaghan [43]. For a review on the various EOSs used see ref. [44]. The bulk modulus B_0 of UAl_2 is found to be higher than that of UAl_3 and UAl_4. Itie *et al* [14] have reported $B_0 = 74$ GPa for UAl_2 which is $\sim 10\%$ lower than this result. The bulk modulus of UAl_3 and UAl_4 are of comparable magnitude.

The higher bulk modulus in UAl_2 is indicative of the itinerant nature of $5f$ states and is consistent with photoelectron spectroscopy results [33]. In UAl_3 and UAl_4, the lower values of bulk modulus may be indicative of localized $5f$ states. However, the low value of bulk modulus is not a sufficient criterion for localized $5f$. There are systems like $NpSn_3$, with B_0 almost similar to UAl_3 and UAl_4, but with itinerant $5f$ states [34]. The reason for itinerant behaviour is attributed to the anisotropic hybridization of the $5f$ states with other orbitals [34]. It is emphasized that conclusions regarding the nature of $5f$ from an isolated measurement may sometimes be misleading [45]. A clear and consistent picture can emerge only by performing the measurements sensitive to electronic structure such as photoemission, Compton scattering and so forth. Band structure calculations would be of

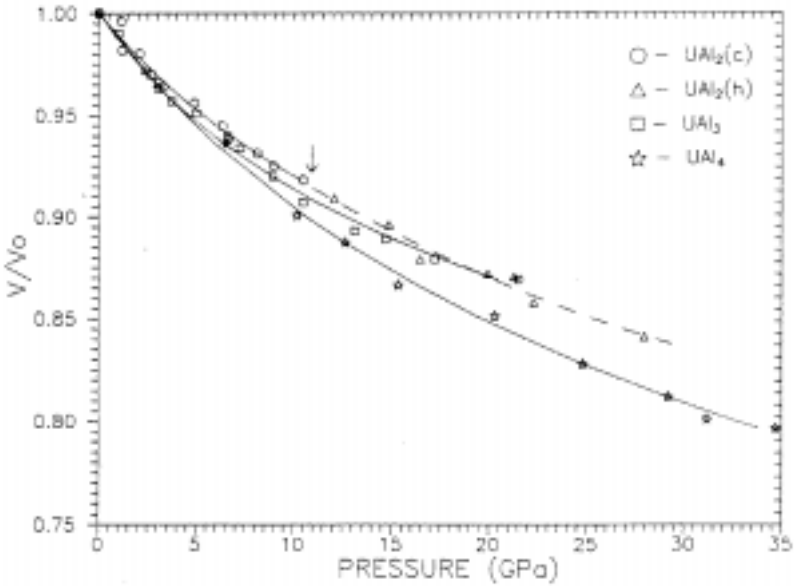

Figure 5. P–V data for UAl_2, UAl_3 and UAl_4. The continuous lines are the Murnaghan fit to the experimental data. In UAl_2, data has been fitted to 11 GPa only [12,13].

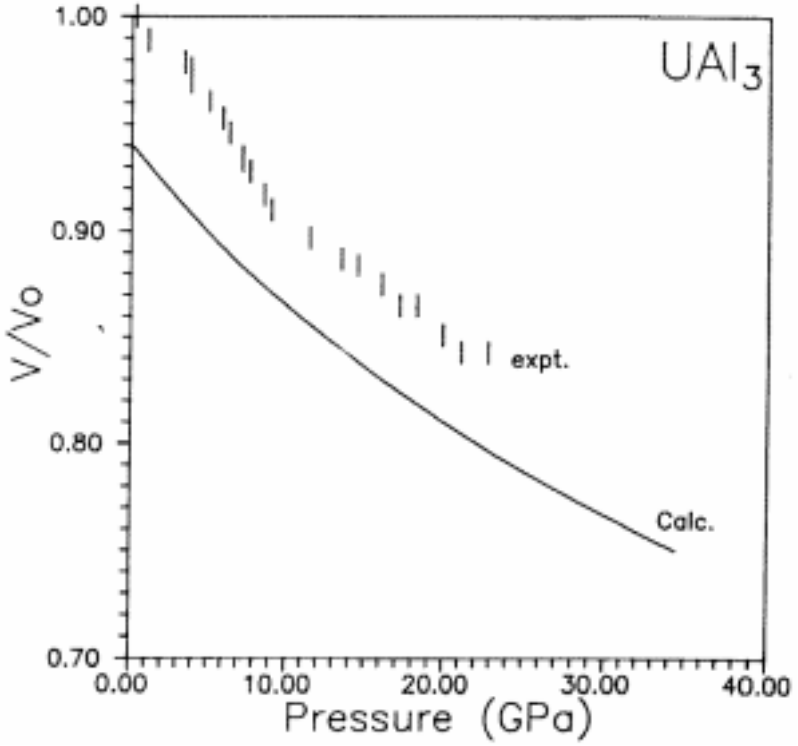

Figure 6. High resolution experimental P–V data for UAl_3 along with the calculated curve. The error bar gives the possible inaccuracies involved in the measurement [40].

Table 2. The bulk modulus B_0 and its pressure derivative B_0' for UAl_2, UAl_3 and UAl_4 obtained by fitting the P–V data to Murnaghan (1st row) and Birch–Murnaghan (2nd row) EOS. For UAl_2, data up to 11 GPa only is used for fitting [13].

Compound	Maximum Pressure (GPa)	B_0 (GPa)	B_0'
UAl_2	28	83.97 ± 7.88	8.10 ± 2.34
		82.39 ± 8.99	9.29 ± 3.55
UAl_3	21	70.08 ± 4.47	9.39 ± 0.89
		66.55 ± 6.65	12.58 ± 2.48
UAl_4	35	74.55 ± 3.97	5.51 ± 0.44
		71.35 ± 4.77	6.60 ± 0.80

much help in determining the nature of $5f$ in these compounds. Such an attempt was indeed made on UAl_3 [40] with an objective to understand the anomaly in the compressibility curve (c.f. figure 6) and to relate it with the nature of its $5f$-electron states.

The band structure and the total energies of UAl_3 which crystallizes in the $AuCu_3$ type structure were obtained by means of the tight-binding linear muffin tin orbital (TB-LMTO) method within the atomic sphere approximation (ASA). The exchange-correlation poten-

tial within the local density approximation (LDA) was calculated using the parametrization scheme of von Barth and Hedin [46]. The most important corrections, namely, the Darwin correction and mass–velocity terms were included, but the spin–orbit coupling was neglected. The calculated compression curve (c.f. figure 6) obtained by fitting the total energies with the Birch–Murnaghan EOS, does not reproduce exactly the features shown by the experimentally observed changes in the slopes. This may be due to the inherent limitations of the present TB-LMTO formalism. The situation may improve if full-potential LMTO (FP-LMTO) method [47] with improved exchange-correlation potential like the generalized gradient approximation (GGA) is employed. The total density of states (DOS) at 1 atmosphere and at two other pressures are presented in figure 7. On compression, a decrease in the total density of states at the Fermi level can be noticed. The band dispersion curves at $V/V_0 = 1$ indicate that the f-electron states extend up to about 1.19 eV below the Fermi level. This is comparable to 1.2 eV of UGe_3 where photoelectron spectroscopy experiments have conclusively shown that f-electrons have a tendency towards localization [48].

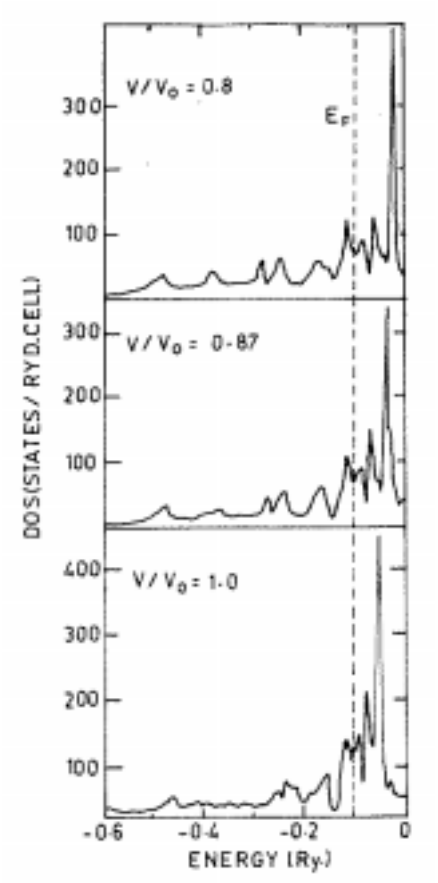

Figure 7. The total electron density of states as a function of energy for UAl_3 computed at various volume compressions. The energies are normalized with respect to the Fermi energy for the equilibrium volume at one atmosphere [40].

Table 3. Partial occupation numbers of s, p, d, f states at the U and Al site in UAl_3 as a function reduced volume [40].

V/V_0	Uranium				Aluminium		
	s	p	d	f	s	p	d
1.0	0.490	0.654	2.276	2.621	1.171	1.503	0.311
0.95	0.483	0.662	2.318	2.587	1.151	1.506	0.326
0.90	0.475	0.670	2.360	2.552	1.130	1.508	0.360
0.85	0.466	0.681	2.404	2.516	1.109	1.508	0.360
0.80	0.457	0.694	2.447	2.483	1.086	1.505	0.382

Upon further compression (c.f. middle and top curves of figure 7), a continuous transfer of electrons from the $5f$ to the $6d$ states at the U site was observed. The partial number of electrons as a function of V/V_0 at both the U and Al sites are given in table 3. From the table, it is clear that the d-like electron concentration at U site increases at the expense of f-like electrons. In summary, the calculations do point out an overall transfer of electrons from $5f$ to $6d$, but are unable to reproduce the changes in the slope of the observed compression curve.

4.1.2. *Phase transition in UAl_2*: Among the dialuminides, UAl_2 exists in the cubic $MgCu_2$ type structure. It was studied earlier by performing high pressure energy dispersive x-ray diffraction with a synchrotron source and a phase transition was observed at $\sim$ 11 GPa [14]. However, the structure of the high pressure phase could not be resolved due to the complicated x-ray diffraction pattern. We accomplished the task by performing high pressure x-ray diffraction experiments using the high resolution Guinier diffractometer [12]. Our experiments confirmed a reversible structural phase transition at around $\sim$ 11 GPa. Figure 8 shows a typical raw diffraction spectra of the parent cubic phase at 1 GPa and the high pressure phase at 25 GPa. Appearance of new peaks and splitting of a few parent peaks indicated that the structure of the high pressure phase might be of lower symmetry. Various possible structures were fitted to the high pressure phase and the best fit was found for the hexagonal, $MgNi_2$ type structure with s.g. $P6_3/mmc$ ($Z = 8$). The lattice parameters at a pressure of $\sim$ 25 GPa were found to be $a = 5.165(15)$ Å, $c = 16.083(15)$ Å and $c/a = 3.114$. Except for the intensities, the calculated interplanar spacings matched very well with the observed values. The discrepancy in intensity can be traced to preferred orientation, a well known feature in HPXRD.

It has been found that almost all the known dialuminides of rare earths and actinides (except for $ThAl_2$) have the Laves phase cubic (C15) $MgCu_2$ type structures with s.g. Fd3m [49, 50]. Apart from the dialuminides, other AB_2 type (A: rare earths, B = Ru, Os, Fe, Co, Ni, etc.) also have this structure [51]. The Laves phases are a set of three related complex structures which occur frequently in AB_2 type binary compounds and are isomorphs of $MgZn_2$ (C14, $Z = 4$). $MgCu_2$ (C15, $Z = 8$) and $MgNi_2$ (C36, $Z = 8$) type structures with similar atomic densities [51–53]. The first and the third structure types are hexagonal with the same space group $P6_3/mmc$, but with different c/a ratios.

The general opinion is that the geometrical factor, viz., the ratio of atomic radii R_A/R_B, plays an important role with the existence of the alloys of the Laves phase type [51,52]. Empirical correlations point out that both the cubic ($MgCu_2$) and hexagonal

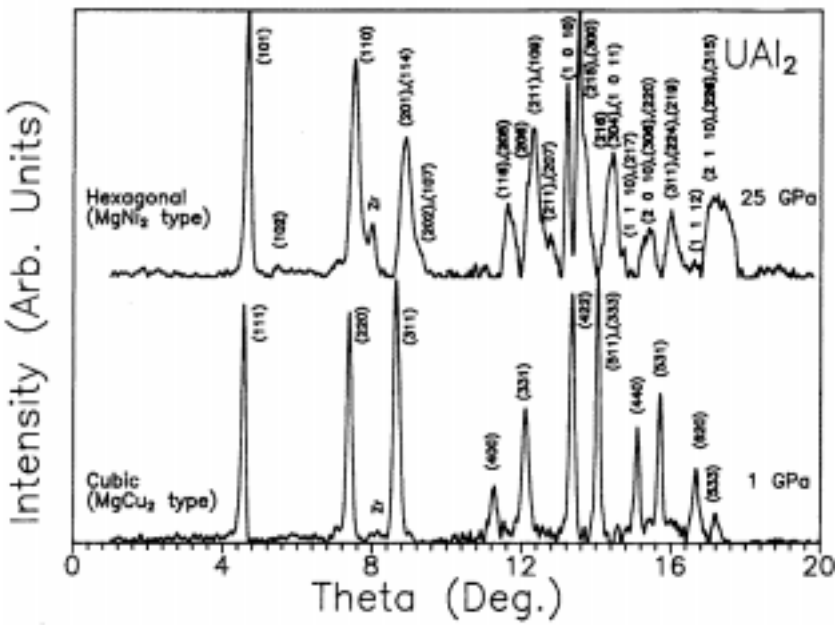

Figure 8. High pressure XRD spectra of UAl_2 at 1 GPa and 25 GPa. The high pressure phase is indexed to $MgNi_2$ type structure [12].

($MgZn_2$ and $MgNi_2$) phases should exist at $R_A/R_B \sim 1.225$. However, in reality, these structures have been found for radii ratios in the range 1.1–1.7. From electronic structure considerations, it has been found that the $MgCu_2$ type structure is stabilized at the free electron concentrations, i.e., the number of free electrons per atom ratio $e/a < 1.8$ and > 2.3 [54,55]. For intermediate concentrations, i.e., $1.8 < e/a < 2.3$, both $MgZn_2$ and $MgNi_2$ structures exist. The interaction between the Fermi surface and the Brillouin zone are considered to be the reason behind the above trend [51]. As the number of free electrons increases, the Fermi surface expands. But when the Fermi surface is on the verge of crossing the Brillouin zone, the system undergoes a phase transition as it is energetically more favourable. The connection between free electron concentration and crystal structure is clearly seen [51] in pseudobinary alloys of type $A(B_{1-x}C_x)_2$ with A = rare earth, B = Al, C = Fe, Co, Ni, etc. The structure is found to change from $MgCu_2$ type to $MgZn_2$ and back to $MgCu_2$ when the concentration of Al increases, in other words, on increasing the free electron concentration from 1 to 3 per atom.

In UAl_2 the e/a ratio is ~ 1.66 [56], which corresponds to the region of stability of $MgCu_2$ type structure. In the f-electron systems under pressure, increased delocalization of the f-electron states leads to an increase in the e/a ratio as well as a decrease in the R_A/R_B ratio due to the contraction of the f electron orbitals of the A atom. Hence in UAl_2 the transition from $MgCu_2$ to $MgNi_2$ type structure can be understood from the increase in the e/a ratio into a region > 1.8 where the $MgZn_2$ or $MgNi_2$ structure are stable. At further higher pressure, it may even transform back to the $MgCu_2$ type structure when its e/a ratio exceeds 2.3. The negligible volume change across the transition in UAl_2 also follows from the almost similar atomic densities of the two structures.

Some of the rare-earth-Os_2 intermetallics like $LaOs_2$, $CeOs_2$ and $PrOs_2$ have also been found to undergo the structural transitions of the type $MgCu_2$ to $MgZn_2$ under pressure [57]. In these systems, the e/a ratios are in the range 1.60–1.68 [56] corresponding to the region of stability of $MgCu_2$ type structure at STP.

Thus it appears that the structural sequence:

$$\mathrm{MgCu_2} \rightarrow \mathrm{MgZn_2(or\ MgNi_2)} \rightarrow \mathrm{MgCu_2}$$

is the natural outcome of the increased delocalization of the f electron states under pressure. This structural sequence can also be expected in other actinide and rare earth based AB_2 type Laves phases with their e/a ratios < 1.8.

4.2 *The $ThAl_2$ system*

$ThAl_2$ exists in the hexagonal AlB_2 type structure [58]. Godwal *et al* [59] investigated this system up to ~ 10 GPa and reported a structural transition from the hexagonal AlB_2 to the cubic $MgCu_2$ type structure at a very low pressure of ~ 0.3 GPa. With an aim to look for a possible sequence in $ThAl_2$, as observed in UAl_2, we studied the system to higher pressures [12,13]. Further details on this work can be found in reference [11].

High pressure x-ray diffraction experiments on $ThAl_2$ were done up to ~ 30 GPa and the P–V data up to 12 GPa is shown in figure 9. In contrast to the earlier report [59]

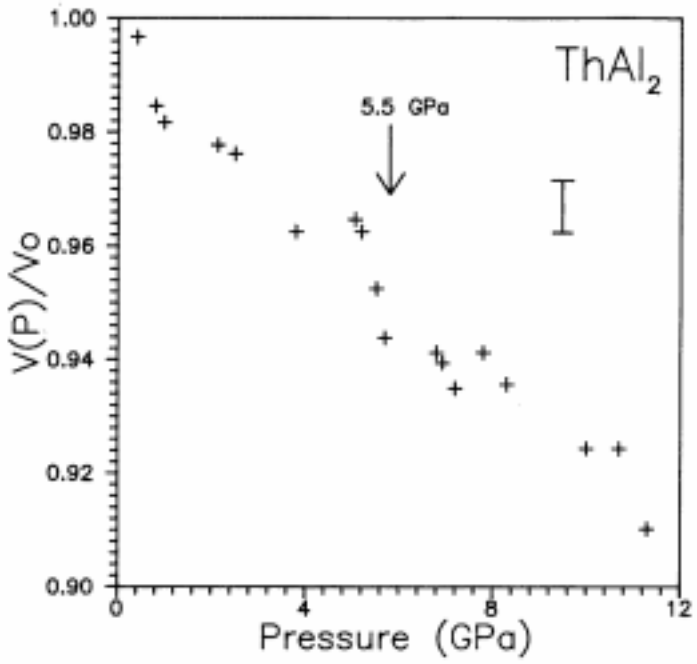

Figure 9. The P–V data of $ThAl_2$ prior to the structural transition. An isostructural transition with a volume change of about 2% at 5 GPa can be noticed. The error bar indicated gives the possible inaccuracies involved in the measurement [11].

it was found that $ThAl_2$ retained its AlB_2 type structure up to a maximum pressure of 12 GPa, where it undergoes a reversible structural transition. Also, it was observed that an isostructural transition, possibly of electronic origin, occurs at around 5.5 GPa. The volume change across the isostructural transition is about 2%. The P–V data of $ThAl_2$ was fitted to the Birch–Murnaghan EOS to obtain the bulk modulus B_0. The value of B_0 obtained in this study is 71 ± 14 GPa up to 5.5 GPa. When the P–V data from 5.5 to 12 GPa were fitted, the value of B_0 obtained was 108 ± 13 GPa.

Figure 10 shows the HPXRD spectra of $ThAl_2$ for AlB_2 (hexagonal) phase at 2 GPa, the isostructural phase at 6.0 GPa, and for the high-pressure phases at 18 and 25 GPa, respectively. At around 12 GPa, the X-ray diffraction pattern of the high pressure phase showed the appearance of new peaks and splitting of the parent peaks indicating that the structure may be of lower symmetry. Using the standard trial and error methods, various structures were tried and best fit was obtained for an orthorhombic lattice. All the peaks at 18 GPa could be indexed to the orthorhombic structure with lattice parameters $a = 5.25 \pm 0.01$ Å, $b = 11.31 \pm 0.01$ Å, and $c = 4.26 \pm 0.01$ Å. The orthorhombic phase remained stable up to 22 GPa. Under further compression, the system goes over to a tetragonal lattice with parameters $a = 4.71 \pm 0.01$ Å and $c = 11.28 \pm 0.05$ Å.

Attempts to fit the high-pressure structures to known space groups and structure types were partially successful. The orthorhombic lattice matched very well with $ZrSi_2$ type

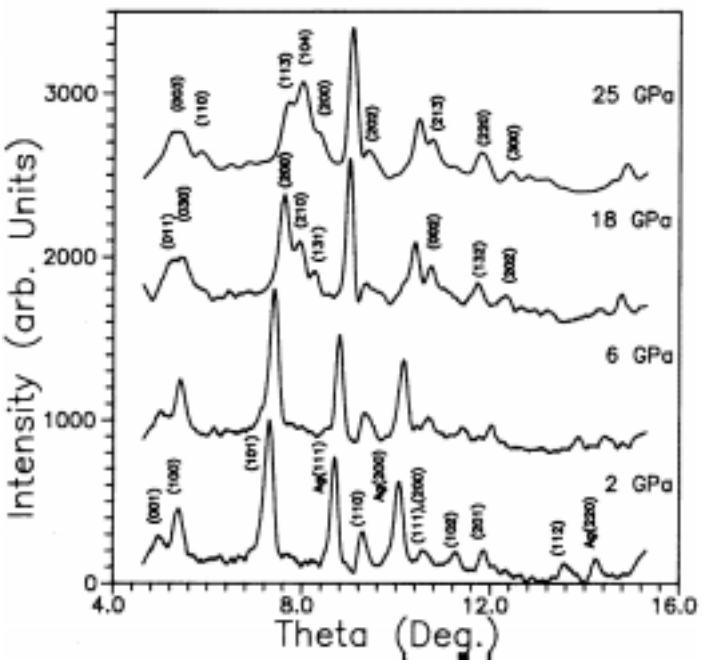

Figure 10. High pressure x-ray diffraction spectra of $ThAl_2$ at 2, 6, 18 and 25 GPa. The pattern at 6 GPa clearly shows that there is no change in the structure above the transition at about 5.5 GPa. The pattern at 18 GPa shows orthorhombic phase and that at 25 GPa the tetragonal phase [11].

structure (s.g. Cmcm) and the tetragonal lattice matched with $ThSi_2$ structure type (s.g. I_4/amd). But a peak-to-peak match with proper intensities was not easy, due to the inherent difficulties with the high-pressure x-ray diffraction patterns, namely, (i) poor resolution and (ii) preferred orientation affecting the intensity distribution.

The observed structural sequence in $ThAl_2$: $AlB_2 \rightarrow ZrSi_2 \rightarrow ThSi_2$ can be visualized geometrically as shown in figure 11. The observed lattice parameters are also consistent with this picture. This structural sequence can be rationalized by considering a reported structural stability map [60] with respect to N, the number of band electrons for the AB_2 type compounds as shown in figure 12. According to this map, the structural sequence starting with the AlB_2 type structure is: $AlB_2 \rightarrow ThSi_2 \rightarrow ZrSi_2$, which is different from the observed sequence. This discrepancy can be explained by considering the interaction of the two types of non-interconnected network of bonded atoms, namely the square lattice and the zigzag chain of atoms found in the $ZrSi_2$ type structure [60]. It is seen that the $ZrSi_2$ type structure is more stable compared to the $ThSi_2$ type if the interaction between these two layers is ignored. In $ThAl_2$, the observation of the $ZrSi_2$ type structure preceding the $ThSi_2$ type structure could be due to a weak interaction of these two network of atoms, as their separation is quite large (2.625 Å). But under pressure, the distance between the two networks decreases resulting in an enhanced interaction. The $ZrSi_2$ structure no more remains stable and transforms to the $ThSi_2$ type structure.

It can be noted from figure 12 that at the beginning of the structural sequence, the distinction between the $MgCu_2$, $MgNi_2$ (or $MgZn_2$) type have not been taken into account. Hence in figure 12 the $MgCu_2$ type structure should be denoted as 'Laves phase' to include the other two Laves phase structures also. In this situation, the structural sequence observed in UAl_2 and $ThAl_2$ seem to be forming part of a greater structure sequence:

$$\mathrm{MgCu_2} \rightarrow \ldots \rightarrow \mathrm{CeCu_2} \rightarrow \mathrm{AlB_2} \rightarrow \mathrm{ZrSi_2} \rightarrow \mathrm{ThSi_2} \rightarrow \mathrm{SmSb_2} \rightarrow \ldots .$$

It is interesting to note that $TmGa_2$ shows a transition from $CeCu_2 \rightarrow AlB_2$ [18] further strengthening the sequence presented in figure 12. It is hoped that at higher pressures $TmGa_2$ may show transition to $ZrSi_2$ or $ThSi_2$ type structures.

At this stage, with limited number of structural phase transformations in the AB_2 type compounds (c.f. table 1), it is not possible to correlate clearly the stability of various structures with the nature and occupancy of their *f*-electron states. Systematic structural studies on more number of compounds as well as electronic structure calculations are essential for accomplishing the above objective.

4.3 *The $CeAl_2$ and $GdAl_2$ systems*

At ambient pressure, both $CeAl_2$ and $GdAl_2$ stabilize in the cubic $MgCu_2$ type structure [55]. $CeAl_2$ is a concentrated Kondo system with approximately integral valence ~ 3 [61]. Anderson's theory predicts that pressure can induce instability of the $4f^1$ shell of Ce^{3+} [62]. Therefore, the onset of strong valence mixing could be established by monitoring the lattice parameter as a function of pressure. The occurrence of a volume anomaly/discontinuity in $CeAl_2$ under pressure has been a point of contention [63–65]. Ramesh and Holzapfel [63] reported an isostructural phase transition in the compound near 7.7 GPa with a volume collapse of about 1%. Earlier reports [64,65] swing between observation of volume collapse of 4% and absence of any discontinuity. The belief

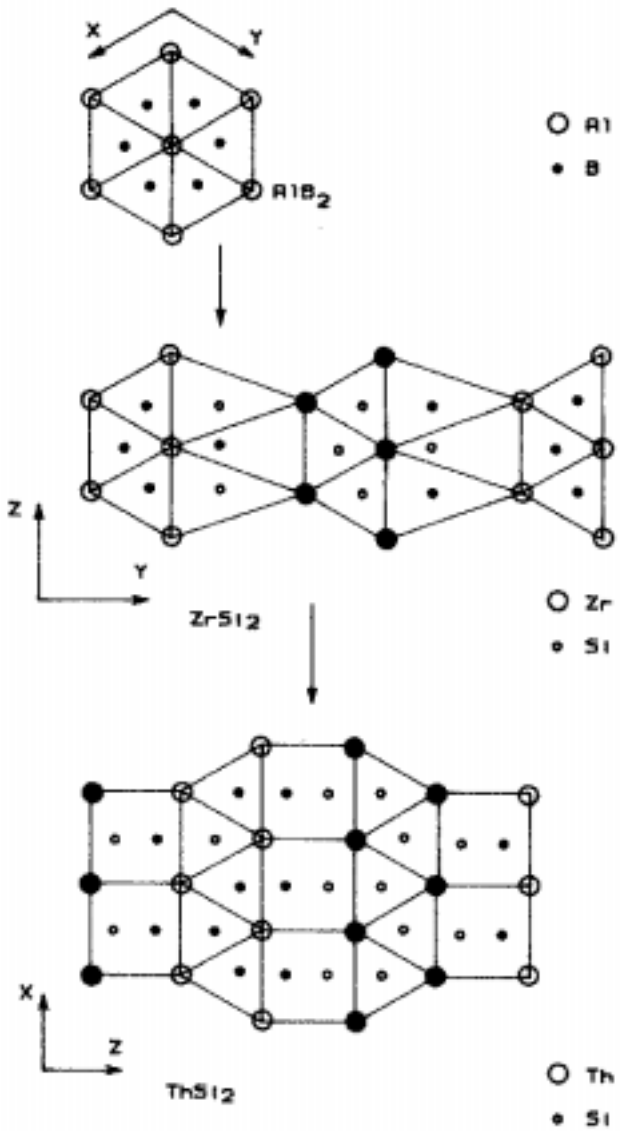

Figure 11. The structural sequence followed by $ThAl_2$ as a function of pressure. The diagram shows the geometric evolution of various structures AlB_2(h) $\rightarrow$ $ZrSi_2$(o) $\rightarrow$ $ThSi_2$(t). The large circles are Al and small circles Th. Open circles are at the origin and closed circles at one half perpendicular to the plane of the paper. $ZrSi_2$ structure type can be regarded as AlB_2 type in which one half of the AlB_2 wall has collapsed and additional Si tetrahedra in-between the AlB_2-like walls (Al in the case of $ThAl_2$). $ThSi_2$ type of structure is also composed of AlB_2-type walls. But the structure is obtained by a screw operation [11].

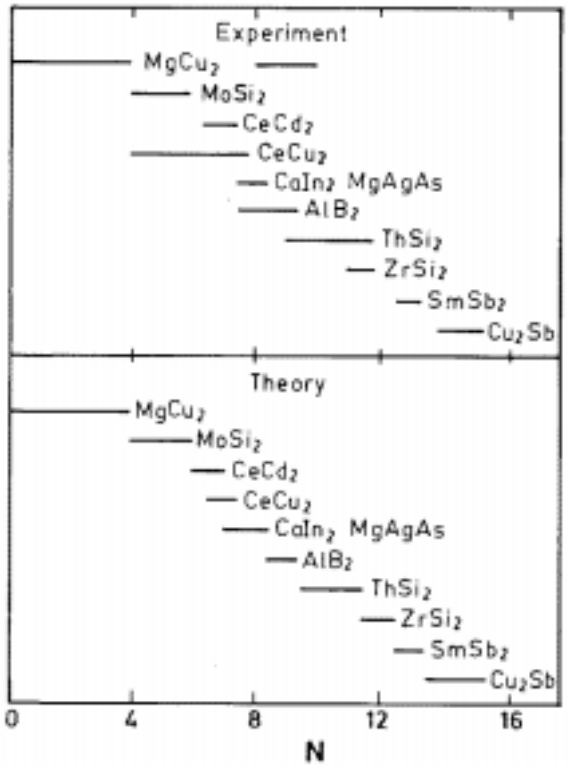

Figure 12. A comparison of the theoretical and experimental ranges of stability with respect to the band filling number N of ten AB_2 type structures [60].

that the anomaly might be linked to the non-hydrostaticity of pressure is not so convincing as similar effects are not noticed in other isostructural compounds [65]. Hence our investigations had two objectives, (i) to look for possible anomaly/discontinuity in the compression curve of $CeAl_2$, and (ii) to compare the compression curve of $GdAl_2$ [15].

4.3.1. *Compressibility behaviour*: High pressure x-ray diffraction experiments were done up to $\sim$ 23 GPa on $CeAl_2$ and up to $\sim$ 16 GPa on $GdAl_2$. Figure 13(a) and (b) show the variation of lattice parameter with pressure. The curves show deviation from normal compressibility behaviour. In the case of $GdAl_2$ (figure 13(b)), the anomaly is very subtle. But $CeAl_2$ shows a significant anomaly between 2–6 GPa (figure13(a)). This continuous and isostructural change observed in $CeAl_2$ is in contrast to a volume collapse observed by other workers [63]. A similar behaviour observed in $AuIn_2$ has been attributed to a Lifshitz transition [66]. The experimental observations point out that the rapid but continuous decrease in volume starts around 2 GPa and ends at $\sim$ 6 GPa and the volume change exhibits a point of inflexion, indicating that the compressibility goes through a maximum. In literature, Lifshitz transition has been considered as a $2\frac{1}{2}$ order transition [67].

The Birch–Murnaghan equation of state, fitted to the P–V curve of $GdAl_2$ gives bulk modulus and its derivative as $B_0 = 69 \pm 5$ GPa and $B_0' = 1.03 \pm 0.6$ respectively

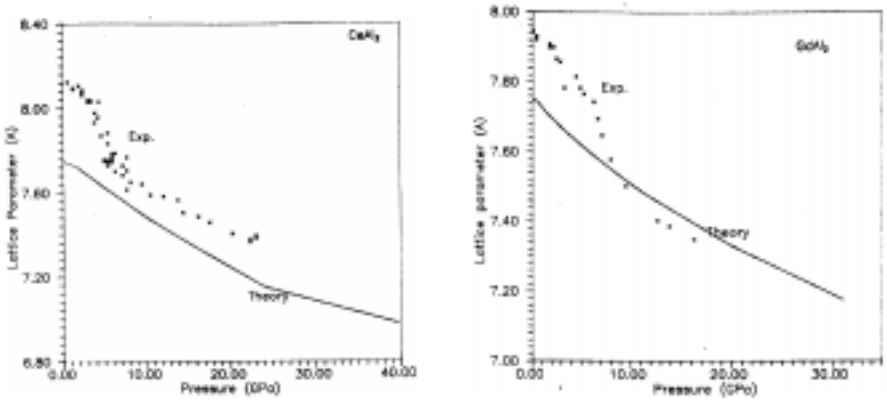

Figure 13. Experimental as well as computed P–V data for $CeAl_2$ (**a**) and $GdAl_2$ (**b**). The pronounced anomaly in the compressibility of the former is evident. The deviation from the normal behaviour is attributed to changes in electronic structure [15].

which is close to those of several other rare earth dialuminides [17]. However, in $CeAl_2$, the P–V data fitted up to 5 GPa yields a bulk modulus of $B_0 = 234 \pm 45$ GPa and $B_0' = -3.7 \pm 9.3$. This shows that $CeAl_2$ is highly incompressible at low pressures (up to ~ 5 GPa) and becomes more compressible at high pressure. Similar behaviour has also been seen in $NpAl_2$ and $NpOs_2$ [68] and has been attributed to the interband transfer of electrons under compression. It may be noted that both in Ce and Np the f-electron states ($4f$ in Ce and $5f$ in Np) are close to the localized itinerant transition zone.

In order to explore the possibility of explaining the compressibility behaviour of these compounds, we have performed band structure calculations. The energy bands of paramagnetic $CeAl_2$ and ferromagnetic $GdAl_2$, which crystallize in the C15 Laves phase, were calculated by means of the TB-LMTO method within the atomic sphere approximation. Our computed compression curves of $CeAl_2$ and $GdAl_2$ (figure 13(a) and (b)) shows changes in the regions corresponding to those observed experimentally. For example in $CeAl_2$, in the pressure range 2–6 GPa, it is observed that some d as well as f bands move across the Fermi level.

It is well known that if the variation of an external parameter, here pressure, causes changes in the Fermi surface topology, it is likely to influence the otherwise monotonic variation of DOS. This was pointed out by Lifshitz [67], who has demonstrated large change in DOS and consequently a change in the associated thermodynamic properties if a closed Fermi surface transforms into an open surface by the formation of a new piece of 'neck'. It was shown by Makarov *et al* [69] for thallium that there is a charge of DOS due to a change in the topology of the Fermi surface which led to a non-linear contribution to the superconducting transition temperature. A similar behaviour was also observed by Chu *et al* for rhenium [70] and Rajagopalan *et al* for phosphorus [71].

In order to look for possible changes in the Fermi surface topology, the energy bands were obtained as a function of pressure. The band dispersion curves for three compressions namely, $0.90V_0$ (5 GPa), $0.875V_0$ (10 GPa) and $0.85V_0$ (14 GPa) are shown in figure 14. At $0.90V_0$ (top curve), the d like band along the symmetry direction $L - \Gamma$ and the f

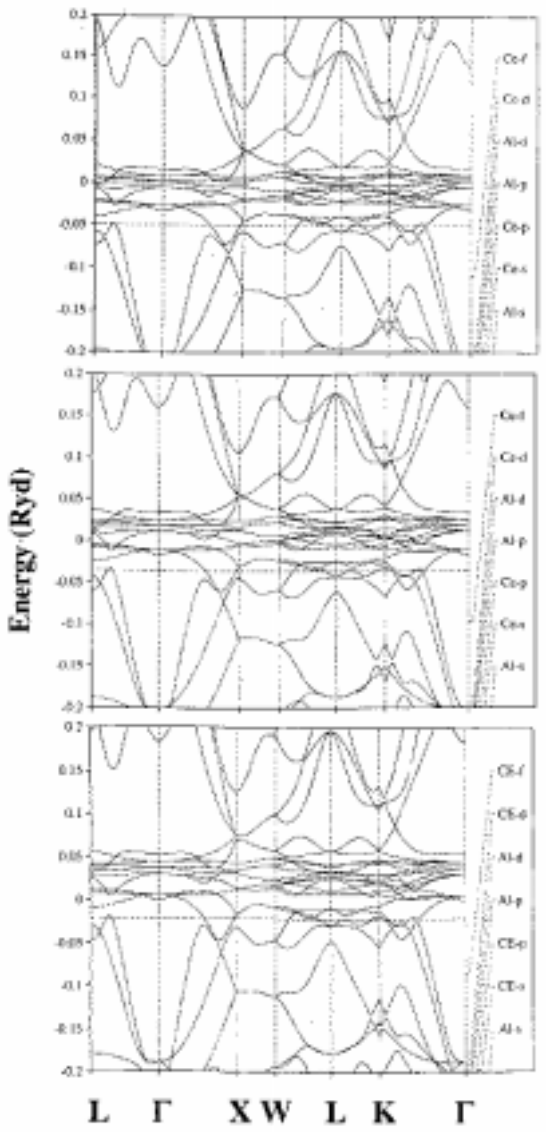

Figure 14. The band dispersion curves of $CeAl_2$ for three compressions namely $0.90V_0$ (top), $0.875V_0$ (middle) and $0.85V_0$ (bottom). The curves show that as a function of pressure, the d like band along $L-\Gamma$ and f-like band along $K-\Gamma$ touch the Fermi level and subsequently cross it [15].

like band along the symmetry direction $K-\Gamma$ just touch the Fermi level. At a compression of $0.875V_0$ (middle curve) the d like band along $L-\Gamma$ and the f like band along $K-\Gamma$ move up and cross the Fermi level, thus causing a change in the topology of the Fermi surface. Upon further compression (bottom curve), these two bands along $L-\Gamma$ and $K-\Gamma$ move

further away from the Fermi level which result in a further fall in the DOS. This change in the Fermi surface topology is reflected in the experimental as well as computed P-V curve. Thus it is tempting to conclude that the electronic transition that is seen in this pressure range could be the cause for the anomaly seen in the compression curve. However, it is to be noted that the computed compressibility curve does not reproduce the steep decrease in volume as observed experimentally. This could be due to the fact that proper $e^- - e^-$ correlation have not been taken into account in the calculation which is expected to have pronounced effect on the compressibility.

Further compression leads to the fall of density of states (DOS) continuously up to $0.75V_0$ (22 GPa). Figure 15 shows the variation of total density of states with pressure. At a compression of $0.70V_0$ (26 GPa) there is a small jump in the DOS. This jump in the DOS is due to the fact that a fd like hybridized band at X point drops down with respect to the Fermi level. The calculated bulk modulus also shows a similar behaviour as the DOS with pressure [15]. This may be an indication of a possible structural phase transition.

5. Structure maps and high pressure phases of intermetallic compounds

Structure maps are used to systematize the occurrence of different structures of compounds [19]. The main objective is to visualize the relationship between the structure type of a compound and the electronic configuration of its constituents, in order to explain the occurrence of observed structure types, and if possible to give some guideline on the possible

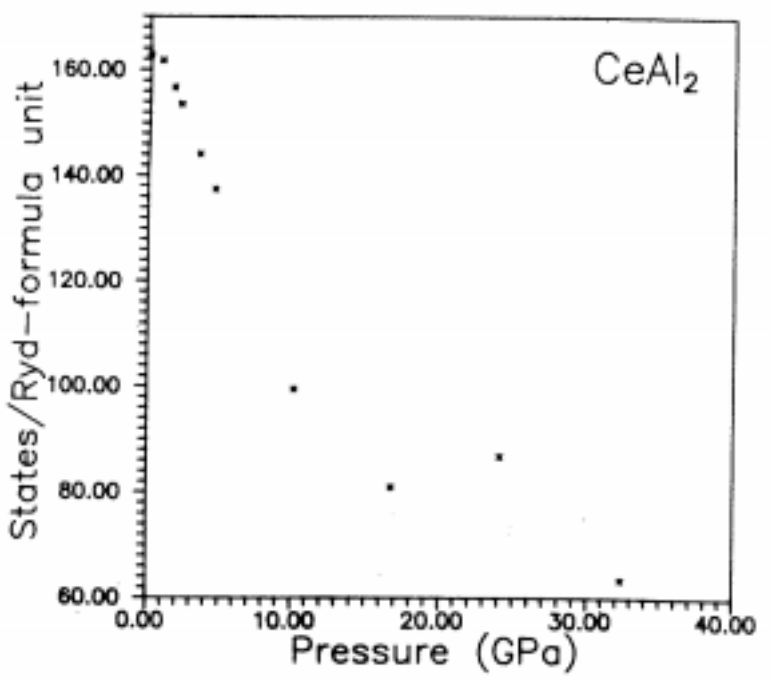

Figure 15. The variation of the total density of states with applied pressure [15].

structure types of new or hypothetical compounds. The quantum mechanical basis for the highly successful microscopic atom model, used with a great degree of accuracy/precision in predicting structural stability of alloys has been reviewed by Pettifor [72].

The use of structure maps in predicting high pressure structural sequence has however not been explored. With several thousands of compounds known, the structure stability maps provide a very important basis for correlating the crystal structure and the electronic configuration of its constituents. As a function of pressure, structural phase transformations are generally a rule rather than exception. Knowledge about possible structures can enormously facilitate the indexing of the x-ray powder diffraction pattern. Recently Villars *et al* [19] have developed structure stability maps for binary compounds based on the three parameters viz.: (i) the average valence electron concentration (VE), (ii) the electronegativity difference (ΔX), and (iii) the pseudo-potential radii difference (ΔR). These are also called three dimensional (or 3D) structure maps. Earlier Pettifor *et al* [73] had developed a 2D structure map. However, Villars' 3D maps are more successful and are able to explain the structure of most of the binary intermetallics. For instance, Pettifor's 2D map predicts cubic $MgCu_2$ type structure for $ThAl_2$ rather than the experimentally observed AlB_2 type structure; whereas the 3 parameter map rightly places the structure as AlB_2.

In the following, the usefulness of Villars' three parameter structural maps in predicting pressure induced structural transitions has been attempted. The parameters VE, ΔX and ΔR for the f electron based AB_2 type compounds undergoing structural phase transitions are listed in table 4. The values for these parameters for the STP phases have been calculated as per the prescription given in ref. [19], whereas for the high pressure phases these values have been inferred from the structure maps. The general decreasing tendency of the various parameters for the high pressure phases can be clearly seen, although there are some ambiguities for VE and ΔX in the case of $ThAl_2$. For $ThAl_2$, the two structures $ZrSi_2$ and $ThSi_2$ have not been considered separately because of their similarity in nature. If the pressure dependence of these three parameters can be computed, then with the help of Villars' structure maps, it will be possible to predict pressure induced structural transitions, and also can aid solving the structures of the high pressure structures.

Table 4. The values of Villars' three parameters: VE, ΔX and ΔR for various phases of UAl_2, $ThAl_2$ and $TmGa_2$.

Compd.	Phases	VE	ΔX	ΔR (Å)	Remarks
UAl_2 [12]	$MgCu_2$ (at STP)	3.0	0.04	2.03	Computed
	$MgNi_2$ (at hp)	2.25–2.74	0	1.00	Inferred from structural map
	$MgCu_2$ (at hp)	2.25–2.74	0	1–0.5	Inferred from structural map
$ThAl_2$ [11]	AlB_2 (at STP)	< 3.33	-0.226	2.203	Computed
	$ZrSi_2$/$ThSi_2$ (at hp)	> 3.33	-0.5 ± 0.5	2.0–1.0	Inferred from structural map
$TmGa_2$ [18]	$CeCu_2$ (at STP)	3.0	-0.33	1.27	Computed
	AlB_2 (at hp)	2.25–2.74	0	2.0–1.0	Inferred from structural map

6. Conclusions and future directions

Our investigations on the f-electron based intermetallics using the high pressure x-ray diffraction technique in the Guinier geometry coupled with TB-LMTO calculations not only produced several interesting results, but also led to several open questions. The compressibility behaviour in UAl_2, UAl_3 and UAl_4 established the decreasing itinerant behaviour of the $5f$-electron states with increasing aluminum concentration. However, these results are to be corroborated with the other experiments like photoelectron spectroscopy, and high pressure and low temperature behaviour of specific heat, magnetic susceptibility and electrical resistivity. Electronic structure calculation is expected to throw more light on this aspect.

The structural transition in UAl_2 and $ThAl_2$ established an interesting structural sequence as a function of band filling number N. More such systems should be studied to establish this structural sequence. Also, these systems should be investigated at further higher pressures using the synchrotron radiation sources to establish and extend the structural sequence.

Interesting isostructural transitions were observed in $ThAl_2$ and $CeAl_2$. Electronic structure calculation on $CeAl_2$ point to a Lifshitz type of transition. Similar calculations should be extended to $ThAl_2$ also. Low temperature specific heat and magnetic susceptibility measurements should be taken up to understand these systems better. Our electronic structure calculation on $CeAl_2$ also indicates another transition in the pressure range 25–30 GPa and requires to be investigated experimentally. We have also attempted to utilize the Villars' 3 parameter structure map in predicting pressure induced structural transitions and understanding the pressure induced evolution of the electronic structure.

Acknowledgements

This review is based on more than half a decade of work carried out in IGCAR, Kalpakkam and we express our gratitude to all who have contributed to this work. We are extremely thankful to Dr. K Govinda Rajan for introducing us to the field of high pressures and to Dr. Mohammad Yousuf, from whom we learnt the high pressure experimental techniques. We are indebted to them for their valuable suggestions and useful discussions. We express our heartfelt gratitude to N Subramanian and M Sekar for their help in this work and to L M Sundaram for his help in sample preparation and characterization. We thank Dr. M Rajagopalan for his collaboration in electronic structure calculations. We convey our thanks to Dr. C S Sundar for critical reading of the manuscript. We thank Dr. T S Radhakrishnan, Dr. Baldev Raj and Dr. Placid Rodriguez for their encouragement and support.

References

[1] A Jayaraman, *Rev. Mod. Phys.* **55**, 65 (1983)
J V Badding, L J Parker and D C Nesting, *J. Solid State Chem.* **117**, 229 (1995)

[2] U Benedict, in *Handbook on the Physics and Chemistry of Actinides* edited by A J Freeman and G H Lander (North Holland, Amsterdam, 1987) vol. 5, p. 227
U Benedict and W B Holzapfel, in *Handbook on the Physics and Chemistry of Rare Earths*

edited by K A Gschneidner Jr, L Eyring, G H Lander and G R Choppin (Elsevier, Amsterdam, 1993) vol. 17, p. 245
[3] P Ch Sahu, N V Chandra Shekar, N Subramanian, Mohammad Yousuf and K Govinda Rajan, in *Advances in High Pressure Research in Condensed Matter* edited by S K Sikka, S C Gupta and B K Godwal (NISCOM, New Delhi, 1997) p. 187
[4] A K McMohan, *Physica* **B139/140**, 31 (1986); *J Less Common Metals* **147**, 1 (1987)
[5] H Tups, K Takemura and K Syassen, *Phys. Rev. Lett.* **49**, 1776 (1982)
A Jayaraman, in *Handbook on the Physics and Chemistry of Rare Earths* edited by K A Gschneidner Jr and L Eyring (North Holland, Amsterdam, 1979) vol. 2, p. 575
[6] K Takemura, in *International Conference on High Pressure Science and Technology* , AIRAPT-17, 25–30 July 1999, Honolulu, Hawaii, p.169
[7] B Johansson and M S S Brooks, in *Handbook on the Physics and Chemistry of Rare Earths* edited by K A Gschneidner Jr, L Eyring, G H Lander and G R Choppin (Elsevier, Amsterdam, 1993) vol. 17, p.1
M S S Brooks, B Johansson and H L Skriver, in *Handbook on the Physics and Chemistry of the Actinides* edited by A J Freeman and G H Lander (North Holland, Amsterdam, 1984) vol. 1, p. 153
[8] J M Fournier and R Troc, in *Handbook on the Physics and Chemistry of the Actinides* edited by A J Freeman and G H Lander (North-Holland, Amsterdam, 1985) vol. 2, p. 29
[9] K Govinda Rajan, *Current Science* **53**, 1115 (1984)
[10] B Johansson, *J. Alloys and Compounds* **223**, 211 (1995)
[11] N V Chandra Shekar, P Ch Sahu, Mohammad Yousuf and K Govinda Rajan, *Phys. Rev.* **B55**, 745 (1997)
[12] P Ch Sahu, N V Chandra Shekar, N Subramanian, Mohammad Yousuf and K Govinda Rajan, *J. Alloys and Compounds* **223**, 49 (1995)
[13] P Ch Sahu, N V Chandra Shekar, N Subramanian, Mohammad Yousuf and K Govinda Rajan, *High Press. Res.* **13**, 295 (1995)
[14] J P Itie, J Staun Olsen, L Gerward, U Benedict and J C Spirlet, *Physica* **B139-140**, 330 (1986)
[15] N V Chandra Shekar, P Ch Sahu, Mohammad Yousuf, K Govinda Rajan and M Rajagopalan, *Solid State Commun.* **111**, 529 (1999)
[16] N V Chandra Shekar, P Ch Sahu, Mohammad Yousuf and K Govinda Rajan, (unpublished)
[17] H Bartholin, F Kervella, A Waintal, G Parisot and J P Senateur, *Phys. Status Solidi* **A6**, K87 (1980)
[18] U Schwarz, S Brauninger, Yu Grin and K Syassen, *J. Alloys and Compounds* **245**, 23 (1996)
[19] P Villars, K Mathis and F Hulliger, in *The Structures of Binary Compounds* edited by F R De Boer and D G Pettifor (North Holland, Amsterdam, 1989) p. 1
[20] P Ch Sahu, Mohammad Yousuf, N V Chandra Shekar, N Subramanian and K Govinda Rajan, *Rev. Sci. Instrum.* **66**, 2599 (1995)
[21] Mohammad Yousuf, in *High Pressure in Semiconductor Physics II, Semiconductors and Semimetals* edited by T Suski and W Paul (Academic Press, San Diego, 1998) vol. 55, ch. 7, p. 381
[22] R Deivasigamani, N Gunasegaran, N Easwaran, Mohammad Yousuf, K V Thomaskutty, P Ch Sahu, N V Chandra Shekar, N Subramanian and K Govinda Rajan, in *Advances in High Pressure Science and Technology* edited by A K Singh (Tata Mc-Graw Hill, New Delhi, 1995) p. 381
[23] L Liu and W A Bassett, *J. Appl. Phys.* **44**, 1475 (1973)
H K Mao, P M Bell, J W Shaner and D J Steinberg, *J. Appl. Phys.* **49**, 3276 (1978)
[24] J D Barnett, S Block and G J Piermarini, *Rev. Sci. Instrum.* **44**, (1973)
G J Piermarini, S Block, J D Barnett and R A Forman, *J. Appl. Phys.* **46**, 2774 (1975)
P M Bell, J Xu and H K Mao, in *Shock Waves in Condensed Matter* edited by Y M Gupta

(Plenum, New York, 1986) p.125
[25] N Subramanian, N V Chandra Shekar, P Ch Sahu, Mohammad Yousuf and K Govinda Rajan, *Phys. Rev.* **B58**, R555 (1998)
[26] J M Fournier, *Solid State Commun.* **29**, 111 (1979)
J M Fournier and E Gratz, in *Handbook on the Physics and Chemistry of Rare Earths* edited by K A Gschneidner Jr, L Eyring, G H Lander and G R Choppin (North-Holland, Amsterdam, 1993) vol. 17, p. 409
[27] R J Trainor, M B Brodsky and H V Culbert, *Phys. Rev. Lett.* **34**, 1019 (1975)
[28] J M Fournier and J Beille, *J. de Phys.* **C4**, 145 (1979)
[29] K H J Buschow and H J van Daal, *AIP Conf. Proc.* **5**, 1464 (1972)
[30] A J Arko, M B Brodsky and W J Nellis, *Phys.Rev.* **B5**, 4564 (1972)
[31] A J Arko, M B Brodsky and W J Nellis, *Bull. Am. Phys. Soc.* **15**, 293 (1970)
[32] H H Hill, in *Plutonium 1970 and other actinides* edited by W N Miner (Metallurgical Society of AIME, New York, 1970) p. 2
[33] R Naegele, L Manes, J C Spirlet, L Pellegrini and J M Fournier, *Physica* **B+C102**, 122 (1980)
J R Naegele, L Manes and J C Spirlet, *Appl. Surf. Sci.* **4**, 510 (1980)
[34] W Potzel, *High Press. Res.* **2**, 367 (1990) and the references cited therein
[35] D D Koelling, B D Dunlop and C W Crabtree, *Phys. Res.* **B31**, 4996 (1985)
[36] M H Van Maaren, H J van Daal, K H J Buschow and C J Schinkel, *Solid State Commun.* **14**, 145 (1974)
[37] A Mielke, W W Kim, G Fraunberger and G R Stewart, *J. Alloys and Compounds* **189**, 123 (1992)
[38] J M Fournier, *Physica* **B130**, 268 (1985)
[39] M S Wire, J D Thompson and Z Fisk, *Phys. Rev.* **B30**, 5591 (1984)
[40] N V Chandra Shekar, P Ch Sahu, M Rajagopalan, Mohammad Yousuf and K Govinda Rajan, *J. Phys. Condens. Matter* **9**, 5867 (1997)
[41] U Benedict, *J. Alloys and Compounds* **223**, 216 (1995)
[42] F D Murnaghan, *Am. J. Math.* **59**, 235 (1937)
[43] F Birch, *Phys. Rev.* **71**, 809 (1947); *J. Geophys. Res.* **57**, 227 (1962)
[44] W B Holzapfel, *High Press. Res.* **16**, 81 (1998)
[45] J M Fournier and L Manes, in *Actinides-Chemistry and Physical Properties-Structure and Bonding* edited by L Manes (Springer-Verlag, Berlin, 1985) vol. 59/60, p. 1
[46] U von Barth and L Hedin, *J. Phys.* **C5**, 1629 (1972)
[47] S Y Savrasov, *Phys. Rev.* **B54**, 16470 (1996)
M Methfessel, *Phys. Rev.* **B38**, 1537 (1988)
[48] A J Arko, D D Koelling and J E Schirber, in *Hand book of Physics and Chemistry of Actinides* edited by A J Freeman and G H Lander (Netherlands, Amsterdam, 1995) vol. 2, p. 175
[49] K H J Buschow, *Rep. Prog. Phys.* **40**, 1179 (1977); **42**, 1373 (1979)
[50] J M Fournier, in *Actinides-Chemistry and Physical Properties – Structure and Bonding* edited by L Manes (Springer, Berlin, 1985) vol. 59/60, p. 127
[51] A Slebarski, *J. Magn. Magn. Mater.* **66**, 107 (1987)
[52] Y Komura and K Tokunaga, *Acta Cryst.* **36**, 1548 (1980)
Y Komura, *Acta Cryst.* **15**, 770 (1962)
[53] B G Hyde and S Andersson, in *Inorganic Crystal Structure* (John Wiley, New York, 1989)
[54] F Laves and H White, *Metallwirtsch Metallwiss. Metalltech.* **14**, 645 (1935); **15**, 840 (1936)
[55] R P Elliot and W Rostoker, *Trans. Am. Soc. Met.* **50**, 617 (1958). P Villars, *J. Less-Common Met.* **92**, 215 (1983)
[56] P Villars, *J. Less Common Metals* **92**, 215 (1983)
[57] J F Cannon, D L Robertson, H T Hall and A C Lawson, *J. Less-Common Met.* **31**, 174 (1973)
[58] P Villars and L D Calvert, in *Pearson's Handbook of Crystallographic Data for Intermetallic*

Phases (ASM, Metals Park, 1991) vol. 1–4
[59] B K Godwal, V Vijayakumar, S K Sikka and R Chidambaram, *Physica* **144**, 44 (1986); *J. Phys.* **F16**, 1415 (1986)
[60] S Lee, *J. Am. Chem. Soc.* **113**, 101 (1991)
[61] H J van Daal and K H J Buschow, *Solid State Commun.* **7**, 217 (1969)
[62] For example, see the papers in *Valence Instabilities and Related Narrow-Band Phenomena* edited by R D Parks (Plenum Press, New York, 1977)
[63] T G Ramesh and W B Holzapfel, *Pramana – J. Phys.* **29**, 183 (1987)
[64] M Croft and A Jayaraman, *Solid State Commun.* **29**, 9 (1979)
[65] I Vedel, A M Redo, J M Leger, J M Mignot and J Flouquet, *J. Magn. Magn. Mater.* **54–57**, 361 (1986)
[66] B K Godwal, A Jayaraman, S Meenakshi, R S Rao, S K Sikka, and V Vijayakumar, *Phys. Rev.* **B57**, 773 (1998)
[67] I M Lifshitz, *Sov. Phys. JETP* **11**, 1130 (1960)
[68] J Zankert, U Potzel, J Moser, W Potzel, T Obenhuber, M Wunsch, G M Kalvius, J Gal and U Benedict, *High Temp.-High Press.* **16**, 533 (1984)
[69] V I Makarow and V G Barlyakhtar, *Sov. Phys. JETP* **21**, 1151 (1965)
[70] C W Chu, T F Smith and W E Gardner, *Phys. Rev.* **B1**, 214 (1970)
[71] M Rajagopalan, M Alouani and N E Christensen, *J. Low Temp. Phys.* **75**, 1 (1989)
[72] D G Pettifor, in *Solid State Physics* edited by H Ehrenreich and D Turnbull (Academic Press, New York, 1987) p. 43
[73] D G Pettifor, *New Scientist* **29**, 48 (1986); *J. Phys.* **C19**, 285 (1986)